A Voltage-Behind-Reactance Synchronous Machine Model for the EMTP-Type Solution

Liwei Wang, *Student Member, IEEE*, and Juri Jatskevich, *Member, IEEE*

***Abstract*—A full-order, voltage-behind-reactance synchronous machine model has recently been proposed in the literature. This paper extends the voltage-behind-reactance formulation for the electromagnetic transient program (EMTP)-type solution, in which the rotor subsystem is expressed in qd coordinates and the stator subsystem is expressed in abc phase coordinates. The model interface with the nodal-analysis network solution is non-iterative and simultaneous. An example of a single-machine, infinite-bus system shows that the proposed model is more accurate and efficient than several existing EMTP machine models.**

***Index Terms*—Computational techniques, electromagnetic transient program (EMTP), phase-domain (PD) model, synchronous machine, voltage-behind-reactance (VBR) model.**

I. Introduction

THERE have been numerous models proposed to represent synchronous machines for power-system analysis. For transient stability studies, reduced-order machine models that neglect stator transients are commonly used [1]. However, for electromagnetic transient studies [2], full-order models are often used, due to their greater accuracy. Depending on the modeling languages, various machine models have been developed using the state-variable approach [3]–[5] (wherein the discretization is performed at the system level by the ODE solver) and the nodal-analysis approach [6], [7] (wherein the discretization is done at the component/branch level using a particular integration rule).

In this paper, synchronous machine models suitable for the electromagnetic transient program (EMTP) solution are investigated. The EMTP and its derivative programs are extensively used by industry and academia as powerful and standard simulation tools, wherein the classical full-order qd synchronous machine model is available.

In the existing EMTP-type software packages, there are three commonly used methods for interfacing the qd machine model with the external network. In the first approach, the machine is represented internally in qd coordinates, but it is interfaced with the external network using a Thevenin equivalent circuit in phase coordinates. The voltage sources of the Thevenin equivalent contain predicted machine electrical and mechanical variables, and the equivalent resistances are averaged to incorporate rotor saliency [8]. A prediction-correction scheme is used for the machine variables, whereas the network variables are solved without iterations. The synchronous machine models Type-50 in MicroTran [9] and Type-59 in DCG/EPRI EMTP [10] fall into this category.

The second approach is based on the compensation method, in which the external ac system is represented as a Thevenin equivalent circuit and is interfaced with the synchronous machine in qd axes. Linear extrapolation of the rotor speed is used at the beginning of each time step. To obtain the solution, iterations are applied to both machine's electrical and mechanical variables. The compensation method works well as long as the distributed-parameter transmission lines separate the machines. When this is not the case, artificial "stub lines" are sometimes used, complicating the network modeling and reducing its accuracy. The universal machine model in the ATP is implemented using this method [11].

In the third method, used in PSCAD/EMTDC [12], the machine model is interfaced with the network as a compensation current source and a special terminating impedance [13]. The machine model is represented as a Norton current source that is calculated using the terminal bus voltages from the previous time step. Therefore, a one-time-step delay exists in this type of machine model.

The key advantage of the qd model is that it uses a constant inductance matrix, making it numerically efficient. Also, the qd model structure makes it possible to incorporate the magnetic saturation in a number of convenient ways [2], [11]. However, the three methods of interfacing the traditional qd machine model with the EMTP network solution artificially reduce simulation efficiency by requiring a small time-step Δt to keep the interfacing error under certain tolerance. When larger time-steps are used, the accuracy of the simulation deteriorates. Moreover, the existing interfacing methods have been shown to cause numerical instability problems [14], [15], which is especially undesirable in real-time simulations [16].

As an alternative to the classical qd model, some researchers have turned to the original coupled-circuit machine model formulation, in which the model is expressed in physical variables and phase coordinates [17]–[21]. In the EMTP community, this approach is known as the phase-domain (PD) model and may provide more accurate representation of machine internal phenomena, such as internal machine faults [20]. Because the stator circuit is directly interfaced to the rest of the network, no predictions and/or iterations of electrical variables are needed and the numerical stability is improved. However, the existence of time-

Manuscript received March 28, 2006; revised July 4, 2006. This work was supported in part by the Natural Science and Engineering Research Council (NSERC) of Canada under the Discovery Grant and in part by the Power Engineering Grant-In-Aid from BC Hydro and Powertech Labs, Inc. Paper no. TPWRS-00172-2006.

The authors are with the Department of Electrical and Computer Engineering, University of British Columbia, Vancouver, BC V6T 1Z4, Canada (e-mail: liweiw@ece.ubc.ca; jurij@ece.ubc.ca).

Color versions of Figs. 3-6 are available online at http://ieeexplore.ieee.org.

Digital Object Identifier 10.1109/TPWRS.2006.883670

variant self and mutual inductances increases the computational burden of this model. Present implementations include Type-58 in ATP [21] (which requires re-triangulation at each time step [22], [23]) and the recently developed VTB model [24].

In order to improve simulation efficiency, a so-called voltage-behind-reactance (VBR) synchronous machine model was proposed in [25] for the state-variable approach. In [26], the VBR synchronous machine model was demonstrated in the hardware-in-the-loop application. This paper extends the VBR model formulation for the EMTP-type solution that is the basis of the real-time power systems simulator at the University of British Columbia [27]. The simulation studies presented provide CPU times and an error analysis that demonstrate the improvement of numerical efficiency and accuracy of the proposed VBR model over several commonly used models, including the PD model. The advantages of the proposed VBR model include the following.

1) Similar to the PD model, the stator circuit is expressed in phase coordinates using the physical currents as the independent variables and is directly interfaced with the external network. A simultaneous EMTP solution is thereby achieved.
2) The rotor equations are expressed in qd-rotor reference frame using flux linkages as the independent variables, which significantly reduces the computational burden as compared to the PD model. The VBR model is also shown to have improved numerical accuracy due to better scaled eigenvalues.
3) The model formulation is very flexible and can be readily extended to include an arbitrary number of electrical phases and/or damper windings.
4) Partitioning of the stator and rotor equations provides a natural decoupling of the time scales. Simulation speed may be further improved through the multi-rate integration [28] and latency techniques [29], which we will investigate in future studies.

II. Synchronous Machine Models

The dynamics of synchronous machines can be represented by equations of corresponding electrical and mechanical subsystems. Without loss of generality, this paper considers a three-phase synchronous machine with one field winding, fd, and one damper winding, kd, in the d-axis, and two damper windings, kq1 and kq2, in the q-axis. Motor convention is used for all models, wherein the q-axis of the rotor reference frame is assumed to be 90° leading the d-axis [30]. Throughout this paper, bold uppercase is used to denote matrices, and bold lowercase is used to denote vectors. Also, the operator $p = d/dt$. The equations for mechanical subsystems are assumed to be the same for all models considered here, specifically

$$p\theta_r = \omega_r \tag{1}$$

$$p\omega_r = \frac{P}{2J}(T_e - T_m). \tag{2}$$

Here, θ_r and ω_r are the rotor position and the angular electrical speed; T_m and T_e are the mechanical torque and electromagnetic torque, respectively. For the purpose of consistency and further discussion, the relevant machine models in their general form are briefly reviewed below.

A. Traditional qd Model

To obtain the qd model, the equations of the coupled-circuit machine model in physical variables are transformed to the rotor reference frame (Park's transformation). The resulting voltage equation, which includes the stator and rotor, may be compactly expressed as

$$\mathbf{v}_{qd0} = \mathbf{R}\mathbf{i}_{qd0} + p\boldsymbol{\lambda}_{qd0} + \mathbf{u} \tag{3}$$

where

$$\mathbf{v}_{qd0} = [\,v_{qs} \quad v_{ds} \quad v_{0s} \quad 0 \quad 0 \quad v_{fd} \quad 0\,]^T \tag{4}$$

$$\mathbf{i}_{qd0} = [\,i_{qs} \quad i_{ds} \quad i_{0s} \quad i_{kql} \quad i_{kq2} \quad i_{fd} \quad i_{kd}\,]^T \tag{5}$$

$$\mathbf{u} = [\,\omega_r\lambda_{ds} \quad -\omega_r\lambda_{qs} \quad 0 \quad 0 \quad 0 \quad 0 \quad 0\,]^T \tag{6}$$

$$\boldsymbol{\lambda}_{qd0} = [\,\lambda_{qs} \quad \lambda_{ds} \quad \lambda_{0s} \quad \lambda_{kq1} \quad \lambda_{kq2} \quad \lambda_{fd} \quad \lambda_{kd}\,]^T \tag{7}$$

$$\mathbf{R} = \begin{bmatrix} \mathbf{R}_s & \\ & \mathbf{R}_r \end{bmatrix}. \tag{8}$$

Here, $\mathbf{v}_{qd0}$ and $\mathbf{i}_{qd0}$ are the vectors of voltages and currents, respectively; v_{fd} represents the field winding voltage; $\mathbf{u}$ includes the speed voltage terms; and $\mathbf{R}$ is a constant diagonal matrix containing the stator and rotor resistances. The flux linkage equations may be expressed as

$$\boldsymbol{\lambda}_{qd0} = \mathbf{L}_{qd0}\mathbf{i}_{qd0} \tag{9}$$

where

$$\mathbf{L}_{qd0} = \begin{bmatrix} \mathbf{L}_{qd0s} & \mathbf{L}_{qd0sr} \\ \mathbf{L}_{qd0rs} & \mathbf{L}_{qd0r} \end{bmatrix}. \tag{10}$$

Note that the inductance matrix, $\mathbf{L}_{qd0}$, does not depend on the rotor position. Finally, the electromagnetic torque is expressed as

$$T_e = \frac{3P}{4}(\lambda_{ds}i_{qs} - \lambda_{qs}i_{ds}). \tag{11}$$

B. Phase-Domain Model

The general form of the PD synchronous machine model is the coupled-circuit model, expressed in physical variables and coordinates. In particular, the voltage equation can be expressed as

$$\begin{bmatrix} \mathbf{v}_{abcs} \\ \mathbf{v}_{qdr} \end{bmatrix} = \mathbf{R}\begin{bmatrix} \mathbf{i}_{abcs} \\ \mathbf{i}_{qdr} \end{bmatrix} + p\begin{bmatrix} \boldsymbol{\lambda}_{abcs} \\ \boldsymbol{\lambda}_{qdr} \end{bmatrix}. \tag{12}$$

The flux linkages are given as

$$\begin{bmatrix} \boldsymbol{\lambda}_{abcs} \\ \boldsymbol{\lambda}_{qdr} \end{bmatrix} = \mathbf{L}(\theta_r)\begin{bmatrix} \mathbf{i}_{abcs} \\ \mathbf{i}_{qdr} \end{bmatrix} \tag{13}$$

with the inductance matrix now depending on the position of the rotor

$$\mathbf{L}(\theta_r) = \begin{bmatrix} \mathbf{L}_s(\theta_r) & \mathbf{L}_{sr}(\theta_r) \\ \mathbf{L}_{rs}(\theta_r) & \mathbf{L}_r \end{bmatrix}. \tag{14}$$

The developed electromagnetic torque is

$$T_e = \frac{1}{2} \begin{bmatrix} \mathbf{i}_{abcs} \\ \mathbf{i}_{qdr} \end{bmatrix}^T \frac{\partial}{\partial \theta_r} \mathbf{L}(\theta_r) \begin{bmatrix} \mathbf{i}_{abcs} \\ \mathbf{i}_{qdr} \end{bmatrix}. \tag{15}$$

The main advantage of this model for the EMTP solution is that the stator circuit is directly integrated with the electrical network, thereby avoiding the interfacing and stability problems common in the qd model. However, the terms dependent on rotor position in (13)–(15) result in an additional computational burden and complexity of the final discretized model.

C. Voltage-Behind-Reactance Model

The VBR formulation decouples the synchronous machine model into stator and rotor subsystems. Since the stator network is interfaced with the EMTP solution, the stator phase currents are used as the independent variables. However, the rotor subsystem is expressed in qd rotor reference frame, with the flux linkages used as the independent variables. A detailed derivation of the VBR model can be found in [25]. For completeness, only the final form suitable for the EMTP solution is given here. In particular, the stator voltage equation can be expressed as

$$\mathbf{v}_{abcs} = \mathbf{R}_s \mathbf{i}_{abcs} + p\left[\mathbf{L}''_{abcs}(\theta_r)\mathbf{i}_{abcs}\right] + \mathbf{v}''_{abcs} \tag{16}$$

where $\mathbf{R}_s$ is a constant diagonal matrix representing stator resistances [26], and $\mathbf{L}''_{abcs}(\theta_r)$ is the so-called subtransient inductance matrix, defined as in (17), shown at the bottom of the page, where

$$L_S(\cdot) = L_{ls} + L_a - L_b\cos(\cdot) \tag{18}$$

$$L_M(\cdot) = -\frac{L_a}{2} - L_b\cos(\cdot) \tag{19}$$

$$L_a = \frac{L''_{mq} + L''_{md}}{3} \tag{20}$$

$$L_b = \frac{L''_{md} - L''_{mq}}{3}. \tag{21}$$

The inductances L''_{md} and L''_{mq} are calculated as

$$L''_{md} = \left[\frac{1}{L_{md}} + \frac{1}{L_{lfd}} + \frac{1}{L_{lkd}}\right]^{-1} \tag{22}$$

$$L''_{mq} = \left[\frac{1}{L_{mq}} + \frac{1}{L_{lkq1}} + \frac{1}{L_{lkq2}}\right]^{-1}. \tag{23}$$

The subtransient voltages $\mathbf{v}''_{abcs}(t)$ in (16) are defined as

$$\mathbf{v}''_{abcs} = \left[\mathbf{K}_s^r(\theta_r)\right]^{-1} \begin{bmatrix} v''_q & v''_d & 0 \end{bmatrix}^T \tag{24}$$

where

$$\begin{aligned} v''_q =& \omega_r \lambda''_d + \frac{L''_{mq} r_{kq1}\left(\lambda''_q - \lambda_{kq1}\right)}{L^2_{lkq1}} \\ &+ \frac{L''_{mq} r_{kq2}\left(\lambda''_q - \lambda_{kq2}\right)}{L^2_{lkq2}} \\ &+ \left(\frac{r_{kq1}}{L^2_{lkq1}} + \frac{r_{kq2}}{L^2_{lkq2}}\right) L''^2_{mq} i_{qs} \end{aligned} \tag{25}$$

$$\begin{aligned} v''_d =& -\omega_r \lambda''_q + \frac{L''_{md} r_{kd}\left(\lambda''_d - \lambda_{kd}\right)}{L^2_{lkd}} + \frac{L''_{md}}{L_{lfd}} v_{fd} \\ &+ \frac{L''_{md} r_{fd}\left(\lambda''_d - \lambda_{fd}\right)}{L^2_{lfd}} \\ &+ \left(\frac{r_{fd}}{L^2_{lfd}} + \frac{r_{kd}}{L^2_{lkd}}\right) L''^2_{md} i_{ds} \end{aligned} \tag{26}$$

with

$$\lambda''_q = L''_{mq}\frac{\lambda_{kql}}{L_{lkq1}} + L''_{mq}\frac{\lambda_{kq2}}{L_{lkq2}} \tag{27}$$

$$\lambda''_d = L''_{md}\frac{\lambda_{fd}}{L_{lfd}} + L''_{md}\frac{\lambda_{kd}}{L_{lkd}}. \tag{28}$$

Rotor dynamics are represented by the following equations:

$$p\lambda_j = -\frac{r_j}{L_{lj}}(\lambda_j - \lambda_{mq}); \quad j = kq1, kq2 \tag{29}$$

$$p\lambda j = -\frac{r_j}{L_{lj}}(\lambda_j - \lambda_{md}) + v_j; \quad j = fd, kd \tag{30}$$

where

$$\lambda_{mq} = L''_{mq}\left(\frac{\lambda_{kq1}}{L_{lkq1}} + \frac{\lambda_{kq2}}{L_{lkq2}} + i_{qs}\right) \tag{31}$$

$$\lambda_{md} = L''_{md}\left(\frac{\lambda_{fd}}{L_{lfd}} + \frac{\lambda_{kd}}{L_{lkd}} + i_{ds}\right). \tag{32}$$

$$\mathbf{L}''_{abcs}(\theta_r) = \begin{bmatrix} L_S(2\theta_r) & L_M\left(2\theta_r - \frac{2\pi}{3}\right) & L_M\left(2\theta_r + \frac{2\pi}{3}\right) \\ L_M\left(2\theta_r - \frac{2\pi}{3}\right) & L_S\left(2\theta_r - \frac{4\pi}{3}\right) & L_M(2\theta_r) \\ L_M\left(2\theta_r + \frac{2\pi}{3}\right) & L_M(2\theta_r) & L_S\left(2\theta_r + \frac{4\pi}{3}\right) \end{bmatrix} \tag{17}$$

Here, λ_j denotes the rotor flux linkages, and λ_{mq} and λ_{md} are the magnetizing flux linkages in qd axes, respectively.

The mechanical equations for the VBR model are identical to (1) and (2). The electromagnetic torque may be calculated as [30]

$$T_e = \frac{3P}{4}(\lambda_{md} i_{qs} - \lambda_{mq} i_{ds}). \tag{33}$$

III. Discrete-Time Model Representations

In order to obtain numerical solutions of the synchronous machine model within the EMTP, the implicit trapezoidal rule is applied to obtain the corresponding difference equations. In particular, discretizing (1) and (2), the difference equations for the rotor position and speed are obtained as

$$\theta_r(t) = \theta_r(t-\Delta t) + \frac{\Delta t}{2}(\omega_r(t) + \omega_r(t-\Delta t)) \tag{34}$$

$$\omega_r(t) = \omega_r(t-\Delta_t) + \frac{\Delta t P}{4J}(T_e(t) + T_e(t-\Delta t)) - \frac{\Delta t P}{2J} T_m \tag{35}$$

which are common to all models considered here. The discretized forms of the qd synchronous machine model [8] are not included in this paper due to space considerations. Instead, the PD and the proposed VBR models are compared, since these two models have similar interfaces with the network. In particular, the general form of these models interfaced into the external network for the EMTP solution can be represented as

$$\mathbf{v}_{abcs}(t) = \mathbf{R}_{eq}(t)\mathbf{i}_{abcs}(t) + \mathbf{e}_h(t) \tag{36}$$

where $\mathbf{R}_{eq}(t)$ is the equivalent resistance matrix (which may need to be inverted) and $\mathbf{e}_h(t)$ is the final history source term.

A. Discrete-Time Phase-Domain Model

Applying the implicit trapezoidal rule with time-step Δt to the voltage (12) gives the following difference equation for the stator voltages of the PD model:

$$\mathbf{v}_{abcs}(t) = \left(\mathbf{R}_s + \frac{2}{\Delta t}\mathbf{L}_s(t)\right)\mathbf{i}_{abcs}(t) + \frac{2}{\Delta t}\mathbf{L}_{sr}(t)\mathbf{i}_{qdr}(t) + \mathbf{e}^{pd}_{sh}(t) \tag{37}$$

where

$$\mathbf{e}^{pd}_{sh}(t) = \left(\mathbf{R}_s - \frac{2}{\Delta t}\mathbf{L}_s(t-\Delta t)\right)\mathbf{i}_{abcs}(t-\Delta t) - \frac{2}{\Delta t}\mathbf{L}_{sr}(t-\Delta t)\mathbf{i}_{qdr}(t-\Delta t) - \mathbf{v}_{abcs}(t-\Delta t). \tag{38}$$

The rotor difference equation can be expressed as

$$\mathbf{i}_{qdr}(t) = \left(\mathbf{R}_r + \frac{2}{\Delta t}\mathbf{L}_r\right)^{-1} \times \left(\mathbf{v}_{qdr}(t) - \frac{2}{\Delta t}\mathbf{L}_{rs}(t)\mathbf{i}_{abcs}(t) - \mathbf{e}^{pd}_{rh}(t)\right) \tag{39}$$

where

$$\mathbf{e}^{pd}_{rh}(t) = \left(\mathbf{R}_r - \frac{2}{\Delta t}\mathbf{L}_r\right)\mathbf{i}_{qdr}(t-\Delta t) - \frac{2}{\Delta t}\mathbf{L}_{rs}(t-\Delta t)\mathbf{i}_{abcs}(t-\Delta t) - \mathbf{v}_{qdr}(t-\Delta t). \tag{40}$$

Substituting (39) into (37), the PD synchronous machine model can be finally interfaced into the external network as

$$\mathbf{v}_{abcs}(t) = \mathbf{R}^{pd}_{eq}(t)\mathbf{i}_{abcs}(t) + \mathbf{e}^{pd}_h(t) \tag{41}$$

where

$$\mathbf{R}^{pd}_{eq}(t) = \mathbf{R}_s + \frac{2}{\Delta t}\mathbf{L}_s(t) - \frac{4}{\Delta t^2}\mathbf{L}_{sr}(t)\left(\mathbf{R}_r + \frac{2}{\Delta t}\mathbf{L}_r\right)^{-1}\mathbf{L}_{rs}(t) \tag{42}$$

and

$$\mathbf{e}^{pd}_h(t) = \mathbf{e}^{pd}_r(t) + \mathbf{e}^{pd}_{sh}(t) \tag{43}$$

with

$$\mathbf{e}^{pd}_r(t) = \frac{2}{\Delta t}\mathbf{L}_{sr}(t)\left(\mathbf{R}_r + \frac{2}{\Delta t}\mathbf{L}_r\right)^{-1}\left(\mathbf{v}_{qdr}(t) - \mathbf{e}^{pd}_{rh}(t)\right). \tag{44}$$

The electromagnetic torque is calculated in phase variables according to (15) or its expended form [30, eq. 5.3-4]. The mechanical subsystem is solved using (34) and (35).

B. Discrete-Time Voltage-Behind-Reactance Model

Discretizing the VBR stator voltage (16) using the implicit trapezoidal rule gives the following equation:

$$\mathbf{v}_{abcs}(t) = \left(\mathbf{R}_s + \frac{2}{\Delta t}\mathbf{L}''_{abcs}(t)\right)\mathbf{i}_{abcs}(t) + \mathbf{v}''_{abcs}(t) + \mathbf{e}^{vbr}_{sh}(t) \tag{45}$$

where

$$\mathbf{e}^{vbr}_{sh}(t) = \left(\mathbf{R}_s - \frac{2}{\Delta t}\mathbf{L}''_{abcs}(t-\Delta t)\right)\mathbf{i}_{abcs}(t-\Delta t) + \mathbf{v}''_{abcs}(t-\Delta t) - \mathbf{v}_{abcs}(t-\Delta t). \tag{46}$$

To interface the VBR model into the external network, (45) should be put into form of (36). Therefore, $\mathbf{v}''_{abcs}$ should be expressed in terms of $\mathbf{i}_{abcs}$. This step can be achieved by discretizing the rotor state equations and solving for the rotor subsystem output variables. After some algebraic manipulation, the difference equations for the rotor flux linkages may be expressed as

$$\begin{bmatrix}\lambda_{kq1}(t)\\ \lambda_{kq2}(t)\end{bmatrix} = \mathbf{E}_1 i_{qs}(t) + \mathbf{E}_2\begin{bmatrix}\lambda_{kq1}(t-\Delta t)\\ \lambda_{kq2}(t-\Delta t)\end{bmatrix} + \mathbf{E}_1 i_{qs}(t-\Delta t) \tag{47}$$

$$\begin{bmatrix}\lambda_{fd}(t)\\ \lambda_{kd}(t)\end{bmatrix} = \mathbf{F}_1 i_{ds}(t) + \mathbf{F}_2\begin{bmatrix}\lambda_{fd}(t-\Delta t)\\ \lambda_{kd}(t-\Delta t)\end{bmatrix} + \mathbf{F}_1 i_{ds}(t-\Delta t) + \mathbf{F}_3 v_{fd}. \tag{48}$$

Here, constant matrices $\mathbf{E}_1$, $\mathbf{E}_2$, $\mathbf{F}_1$, $\mathbf{F}_2$, and $\mathbf{F}_3$ are due to the qd transformation and are given in Appendix A. Further, substituting (47), (48), (27), and (28) into the rotor output (25) and (26), $\mathbf{v}''_{qd}$ may be expressed as

$$\mathbf{v}''_{qd}(t) = \begin{pmatrix} \mathbf{k}_1(\omega_r) & \mathbf{k}_2(\omega_r) \end{pmatrix} \mathbf{i}_{qds}(t) + \mathbf{h}_{qdr}(t). \tag{49}$$

Here, $\mathbf{k}_1(\omega_r)$ and $\mathbf{k}_2(\omega_r)$ are vectors that depend on the rotor speed ω_r; $\mathbf{h}_{qdr}$ is equivalent history source, including the excitation voltage and the history values of the stator currents and the rotor flux linkages, respectively. These variables are also defined in Appendix A.

After $\mathbf{v}''_{qd}$ and $\mathbf{i}_{qdr}$ are transformed into abc phase coordinates, the subtransient voltages $\mathbf{v}''_{abcs}$ are expressed as

$$\mathbf{v}''_{abcs}(t) = \mathbf{K}(t)\mathbf{i}_{abcs}(t) + \mathbf{e}_r^{vbr}(t) \tag{50}$$

where

$$\mathbf{K}(t) = [\mathbf{K}_s^r(\theta_r)]^{-1} \begin{bmatrix} \mathbf{k}_1(\omega_r) & \mathbf{k}_2(\omega_r) & 0_{2\times 1} \\ 0 & 0 & 0 \end{bmatrix} \mathbf{K}_s^r(\theta_r) \tag{51}$$

and

$$\mathbf{e}_r^{vbr}(t) = [\mathbf{K}_s^r(\theta_r)]^{-1} \begin{bmatrix} \mathbf{h}_{qdr}(t) \\ 0 \end{bmatrix}. \tag{52}$$

Finally, substituting (50) into (45), the VBR model can be interfaced into the external network as

$$\mathbf{v}_{abcs}(t) = \mathbf{R}_{eq}^{vbr}(t)\mathbf{i}_{abcs}(t) + \mathbf{e}_h^{vbr}(t) \tag{53}$$

where

$$\mathbf{R}_{eq}^{vbr}(t) = \mathbf{R}_s + \frac{2}{\Delta t}\mathbf{L}''_{abcs}(t) + \mathbf{K}(t) \tag{54}$$

and

$$\mathbf{e}_h^{vbr}(t) = \mathbf{e}_r^{vbr}(t) + \mathbf{e}_{sh}^{vbr}(t). \tag{55}$$

Similar to the PD model, the rotor position and speed are calculated using (34) and (35). However, the electromagnetic torque, T_e, is calculated using (33).

C. Model Complexity

The difference equations of the PD and VBR models have similar forms, since (41)–(43) are analogous to (53)–(55). However, the computational cost associated with these equations is substantially different. The number of floating point operations (flops) required to complete the calculations is often used as a measure of numerical complexity and/or efficiency of a given algorithm. Here, we use the definition of a flop as one addition, subtraction, multiplication, or division of two floating-point numbers [31]. The number of flops for one trigonometric function (trig) evaluation (cos or sin) depends on the floating-point-unit (FPU) processor and/or internal implementation and may cost several flops. After very careful evaluation of the model equations (taking into account that many coefficients and terms can be precalculated and stored for better speed), the number of flops and trigs for the PD and VBR models are summarized in Table I. The total number of flops is also roughly divided among the different terms/equations to better understand where the computational enhancement is achieved.

TABLE I
FLOPS AND TRIG FUNCTIONS COUNT PER TIME STEP

PD Model			VBR Model		
$\mathbf{L}_s(\theta_r)$ $\mathbf{L}_{sr}(\theta_r)$ $\mathbf{L}_{rs}(\theta_r)$	flop	trig	$\mathbf{L}''_{abcs}(\theta_r)$ $\mathbf{K}_s^r(\theta_r)$ $[\mathbf{K}_s^r(\theta_r)]^{-1}$	flop	trig
	33	9		20	9
$\mathbf{R}_{eq}^{pd}$	96	-	$\mathbf{R}_{eq}^{vbr}$	76	-
$\mathbf{e}_h^{pd}$	280	-	$\mathbf{e}_h^{vbr}$	105	-
$\mathbf{i}_{qdr}$	76	-	$\boldsymbol{\lambda}_{qdr}$	46	-
T_e^{pd}	62	1	T_e^{vbr}	4	-
Total	546	10	Total	241	9

As can be seen in Table I, a significant number of flops is spent on computing the history terms $\mathbf{e}_h^{pd}$ and $\mathbf{e}_h^{vbr}$. Because the VBR model utilizes qd transformation for the rotor part, most of the terms and/or coefficients in the discretized rotor (47)–(49) are constant and therefore precalculated outside and before the major time step loop. At the same time, many of the terms and/or equations in the PD model contain time-variant coefficients that must be recalculated due to changing inductances. Another significant saving is achieved in calculating the electromagnetic torque using (33) instead of (15). The difference in the total number of flops will further increase to the benefit of VBR model if one considers a synchronous machine with larger number of damper windings (e.g., 6 in [25]). This can be clearly observed as the dimensions of matrices $\mathbf{L}_{sr}(\theta_r)$, $\mathbf{L}_{rs}(\theta_r)$, and $\mathbf{L}_r$ will increase for the PD model, which further increases the computational costs. However, the dimensions of $\mathbf{L}''_{abcs}(\theta_r)$, $\mathbf{K}_s^r(\theta_r)$, $[\mathbf{K}_s^r(\theta_r)]^{-1}$ do not change, and there will be less of an increase in the number of flops for the VBR model.

IV. INTERFACE PROCEDURE

The method used for interfacing the VBR synchronous machine model is similar to that of the PD model. In particular, the machine is connected to the external network as a three-phase Thevenin equivalent circuit, as shown in Fig. 1. Without loss of generality, the machine windings are assumed to be Y-connected, with the neutral grounded, although any other connection of windings is possible. The sequence of calculation steps in interfacing the VBR model is briefly described here, assuming that the solution at time-step $t - \Delta t$ is known and that the solution at t is to be found.

1) *Predict the mechanical variables:* As the mechanical equations are nonlinear, the exact and simultaneous solution of the mechanical and electrical variables, in general, would require iterations. However, since the me-

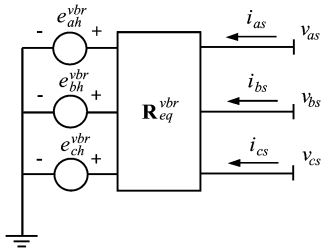

Fig. 1. Thevenin equivalent circuit of the proposed VBR model.

chanical variables change relatively slowly compared to the electrical variables, the linear extrapolation of θ_r and ω_r used in [2] and [20] is also applied here as

$$\theta_r(t) = 2\theta_r(t-\Delta t) - \theta_r(t-2\Delta t) \quad (56)$$

$$\omega_r(t) = 2\omega_r(t-\Delta t) - \omega_r(t-2\Delta t). \quad (57)$$

2) *Form the Thevenin equivalent circuit:* (54) and (55) are evaluated to assemble the Thevenin equivalent circuit of the synchronous machine.
3) *Solve the network equations:* The network conductance matrix $\mathbf{G}$ is triangularized, and the network variables are solved.
4) *Update machine's stator and rotor variables:* Stator currents and rotor flux linkages are calculated according to (53), (47), and (48). Subtransient voltages $\mathbf{v}''_{abcs}$ and equivalent history terms are also calculated by (50), (46), and (52).
5) *Update the machine's mechanical part:* The electromagnetic torque T_e is calculated using (33). Then, the rotor displacement θ_r and speed ω_r are recalculated using (34) and (35).

V. Computer Studies

A single-machine, infinite-bus case system is assumed here to compare the different models. The machine parameters obtained from [30] are summarized in Appendix B. To validate the proposed VBR model, the case system has been implemented using various simulation packages, including MicroTran, ATP, and MATLAB/Simulink. In the transient study considered here, the machine initially operates in an idle steady-state mode with load torque $T_m = 0$, and the nominal excitation is kept constant. At $t = 0$, a symmetric three-phase fault is applied at the machine terminals. The dynamic responses produced by various models using different time steps are plotted in Figs. 2 and 3. The studies of unbalance operations are discussed in [32].

A. Model Verification

Fig. 2 depicts the fault transient observed in the field current i_{fd}, a-phase current i_{as}, and the electromagnetic torque T_e. Other variables are not shown due to space limitations. Since the analytical solution is not available, a reference solution was obtained using the qd model implemented in MATLAB/Simulink (state-variable approach) and solved with the Runge–Kutta fourth-order method with an integration time-step $\Delta t = 1$ μs. This solution is considered a trustworthy reference because it was obtained with a high-order method

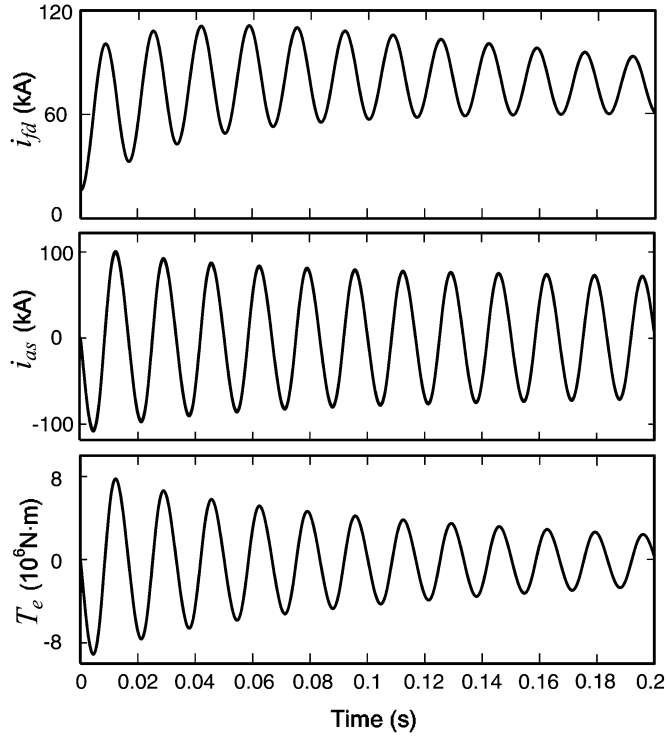

Fig. 2. Simulation results with time-step of 50 μs.

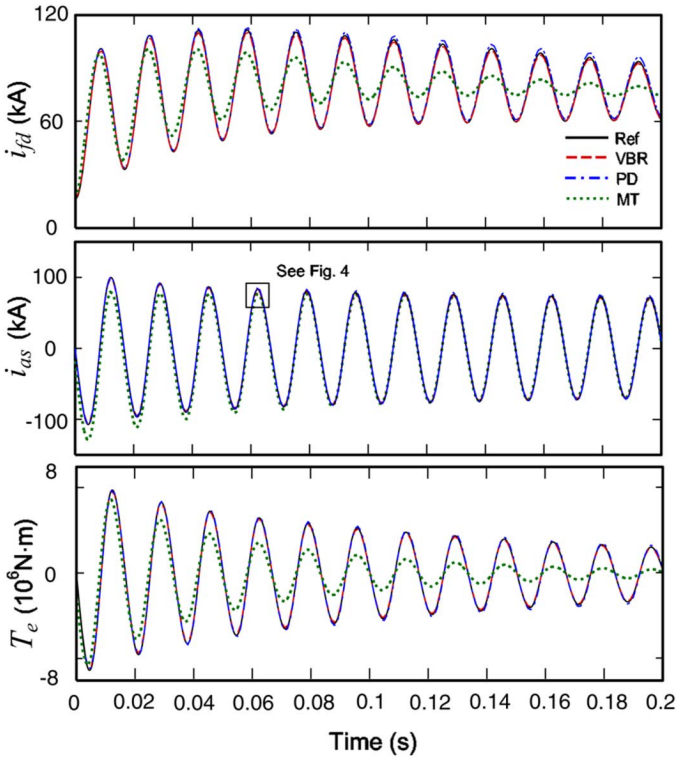

Fig. 3. Simulation results with time-step of 1 ms.

using a very small time-step. The same transient study was reproduced by different models using the time-step $\Delta t = 50$ μs. The corresponding results are superimposed with the reference solutions in Fig. 2, wherein it is shown that the responses

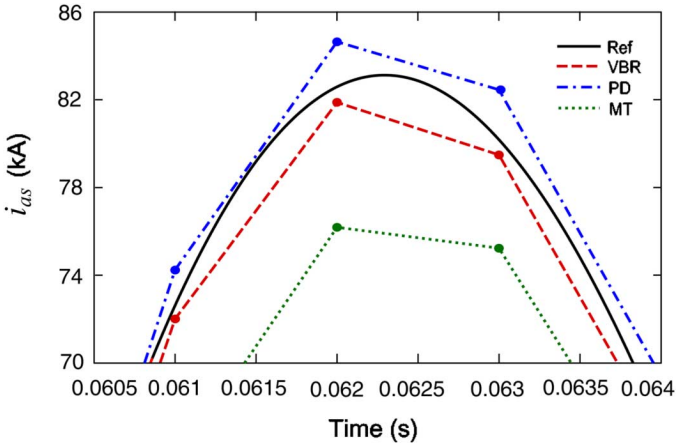

Fig. 4. Detailed view of the portion of i_{as} with the time-step of 1 ms.

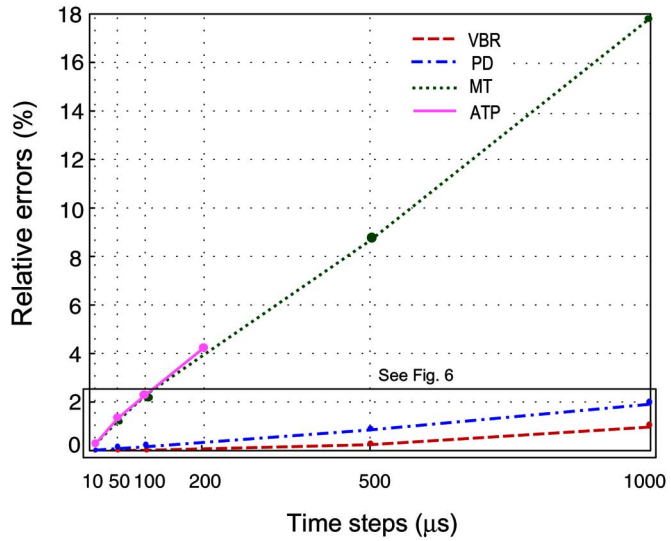

Fig. 5. Propagation of numerical errors in i_{as}.

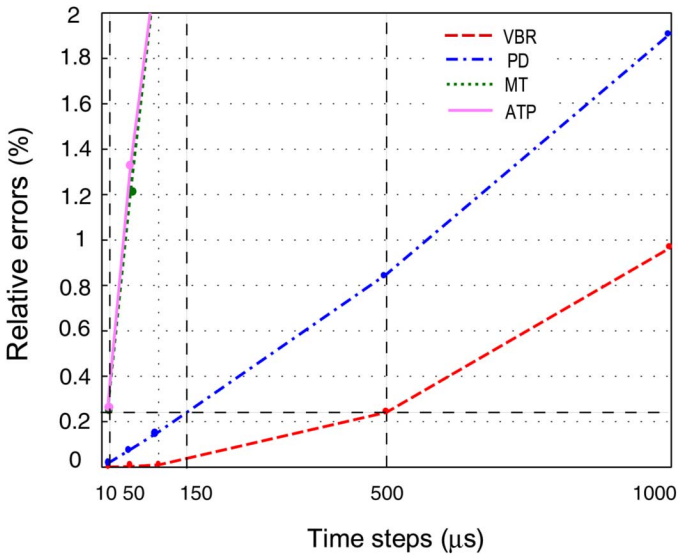

Fig. 6. Comparison of time-steps and numerical errors in i_{as}.

predicted by the above-mentioned models are visibly indistinguishable from the reference solution and each other. This result indicates that the qd model, the PD model, and the VBR model are all equivalent despite the different simulation languages and integration methods used. This study also validates the proposed VBR model.

B. Numerical Accuracy

Although the simulation results obtained by different models are all convergent to the reference solution when the step size is small, error between the solutions still exists. To study the error behavior and stability of different models, the same simulation study was run with different integration time steps. An example study performed with a larger time-step ($\Delta t = 1$ ms) is shown in Fig. 3, wherein the general trend of error produced by different models can be observed. Here, and in other figures, the legend MT denotes the results obtained using MicroTran. Studies with other time-steps are not included due to space limitations. Fig. 3 shows that at such a large time-step, the MicroTran's Type-50 machine model (see dotted-line MT) has a large error, while the ATP Type-59 model was no longer convergent. This behavior is mainly due to the interface of the qd model with the external network, which quickly deteriorates the simulation accuracy as the time-step increases. At the same time, the PD and VBR models remain stable at this large Δt and still produce results reasonably close to the reference solution. To see the details among the simulation results produced by the stable models, a fragment of the peak of current i_{as} is shown in Fig. 4. As can be seen, the solution points obtained by the VBR model are closer to the reference solution than the results of either the PD model or the MT model.

To evaluate the accuracy of different numerical solutions, a relative error between the reference solution trajectory and a given numerical solution may be considered. The relative error is calculated here using the 2-norm [33] as

$$\%\text{error} = \frac{||\widetilde{\mathbf{f}} - \mathbf{f}||_2}{||\mathbf{f}||_2} \times 100 \tag{58}$$

where $\mathbf{f}$ denotes the reference solution and $\widetilde{\mathbf{f}}$ is the numerical solution. Without loss of generality, the relative error was calculated for one variable only, stator current i_{as}, since the error of the other variables is similar. The error was calculated for different time-step sizes. The results for the different models are shown in Figs. 5 and 6.

As can be seen in Fig. 5, the PD and the VBR models are all noticeably more accurate than the qd models of MicroTran and ATP. In particular, when the time-step Δt is larger than 0.2 ms, the MicroTran's qd model will have an error exceeding 4%, and the ATP's qd model is no longer convergent. Although the qd model implemented in MicroTran appears to be stable even after $\Delta t = 0.2$ ms, the large error observed in other variables (see Fig. 3, i_{fd} and T_e) supports the conclusion that the traditional qd models should preferably be used with small step size and with caution.

TABLE II
COMPARISON OF CPU TIMES

CPU times	PD Model	VBR Model
0.2s study	0.031s	0.015s
Per time-step	7.75μs	3.75μs

C. Model Efficiency

The proposed VBR and PD models were both implemented in standard C language and compiled for the purpose of benchmark comparisons. The compiled models were executed on a personal computer (PC) with a Pentium 4, 2.66-GHz processor and 512M RAM. The CPU times required by the two models for the 0.2-s case study with the integration time-step $\Delta t = 50\ \mu$s are summarized in Table II. It can be seen that although both models can realize a faster than real-time simulation speed, the proposed VBR model achieves a roughly 200% improvement of simulation speed over the PD model. This result is very much consistent with the flops count provided in Table I for the two models.

To compare the overall simulation efficiency, some common error tolerance should be assumed. Herein, a relative error tolerance of 0.25% is considered. To achieve this tolerance, MicroTran's and ATP's qd models require a time-step $\Delta t = 10\ \mu$s, and the PD model needs a time-step $\Delta t = 150\ \mu$s, as shown in Fig. 6. However, the proposed VBR model may use the time-step as large as 500 μs, which outperforms the PD model by 3.3 times and the traditional qd models by about 50 times. Altogether, taking into account the CPU times in Table II, the VBR model demonstrates a 660% improvement over the PD model for the same relative tolerance of 0.25%.

VI. ERROR ANALYSIS

It is important to point out that the standard qd model, the PD model, and the VBR model are all equivalent for continuous-time analysis since no approximation is made when these models are algebraically derived from each other. However, when these models are discretized using a specific integration rule and interfaced into the EMTP network solution, their numerical properties are different.

As shown in Figs. 5 and 6, the qd models (MT and ATP) quickly lose accuracy compared to the PD and the VBR models. Such behavior is due to the interface of the qd models and the prediction of fast electrical variables such as stator currents and speed voltages [2].

The accuracy of PD and VBR models should be examined in more detail. As was shown in [25], the choice of independent variables and the structure of the model change the system's eigenvalues, which are linked to the accuracy and performance of different numerical solvers.

To achieve the EMTP solution, the PD and VBR models are discretized using the same implicit trapezoidal integration rule as described in Section III. To further compare the numerical property of these two models, the corresponding difference equations should be analyzed. Since the trapezoidal rule is a one-step integration scheme, the model equations may be expressed in the form of a one-step update formula as [33]

$$\mathbf{x}_n = \mathbf{\Phi}(\Delta t, t, \mathbf{x}_{n-1})\mathbf{x}_{n-1} + \mathbf{f}(\Delta t, t). \tag{59}$$

TABLE III
EIGENVALUES OF MACHINE MODELS

Continuous Time		Discrete Time	
PD	VBR	PD	VBR
954.2	32.0+j26.4	0.395	0.945-j0.028
890.3	32.0-j26.4	0.418	0.945+j0.028
-4.2	-0.88	0.976	0.994
-6.00	-5.39	0.994	0.995
-24.2	-5.96	0.996	0.999
-904.6	-57.3+j30.6	2.358	1.031-j0.027
-968.3	-57.3-j30.6	2.498	1.031+j0.027

Here, the vector $\mathbf{x}$ contains combined independent variables (currents and/or flux linkages); $\mathbf{f}(\Delta t, t)$ represents the forcing function that includes the terminal voltages, $\mathbf{v}_{abcs}$, and the excitation voltage, v_{fd}. Thereafter, the numerical behavior and the local error propagation can be related to the eigenvalues of the update matrix $\mathbf{\Phi}(\Delta t, t, \mathbf{x}_{n-1})$, as this matrix directly relates the present step solution (error) to the next step solution (error). After extensive algebraic manipulations with the equations of Section III, both PD and VBR models can be put into the form of (59). Only the final update matrices $\mathbf{\Phi}^{pd}\left(\Delta t, t, \mathbf{x}_{n-1}^{pd}\right)$ and $\mathbf{\Phi}^{vbr}\left(\Delta t, t, \mathbf{x}_{n-1}^{vbr}\right)$ are given in Appendix A. The corresponding discrete-time eigenvalues are calculated for $\Delta t = 1$ ms and summarized in Table III. For consistency, the continuous-time eigenvalues were also calculated using the methodology described in [25] and are included as well.

It is interesting to note that although both PD and VBR models have rotor-position-dependent terms, the respective systems have time-invariant eigenvalues due to the machine symmetry. Another important observation is that both models, when expressed in continuous time, have some eigenvalues with positive real parts. Contrary to the linear time-invariant systems, positive eigenvalues do not imply instability of the time-varying systems [34]. Although it is preferable to have eigenvalues with negative real part, the existence of positive eigenvalues may increase the propagation of local errors when a particular numerical solution scheme is used [35]. In this regard, the positive eigenvalues of the VBR model are much smaller than those of the PD model, which indicates a potentially better numerical conditioning of the VBR model.

When the models are discretized, the eigenvalues of the corresponding difference equation (59) should be compared against the unit circle on the complex plane. Here, by analogy with continuous-time systems, the eigenvalues outside of the unit circle do not imply the system's instability, because both models are time-varying. However, for numerical considerations, it is desirable to have the eigenvalues inside the unit circle (or closer to the origin). In this regard, the magnitude of the largest eigenvalue of the VBR model (1.031) is roughly two times smaller than the largest eigenvalue of the PD model (2.498). This observation again indicates a better numerical conditioning of the VBR model and is completely consistent with the relative error results shown in Figs. 5 and 6.

VII. DISCUSSION OF NETWORK SOLUTION

Although the focus of this paper is the VBR synchronous machine model, it is also of interest and importance to develop an efficient network solution approach to integrate the VBR machine model in EMTP-type programs. Similar to the PD model,

the VBR machine model introduces time-varying elements in the network conductance matrix, which may lead to an increase of the execution time if the entire network conductance matrix is re-factorized at each time step (see step 3, Section IV). Some case studies presented in [14] compare the calculation times and the number of triangulations when using Type-58 (PD model) and Type-59 (qd model) synchronous machine models, respectively. For a 190-bus three-generator system, the ratio of 308.3/70.1 (about 4.4 times) of increased calculation time due to re-triangulation was reported [14, Table I].

The impact of time-varying elements on the efficiency of EMTP solution depends on the relative proportion of machines verses other components and the overall system size [36]. If there are only one or a few synchronous machines in the network, the extra computation effort can be reduced by using the compensation method [2]. To get an idea about the increase in execution time with the compensation method, the IEEE First Benchmark Model for SSR [37] was considered, wherein an increase by about 15% per-time-step was observed. Another method is to place the nodes with synchronous machines as the last nodes in the nodal equations and triangularize first the upper part of the conductance matrix before the time-step loop starts. That will produce a small lower sub-matrix [38, Fig. 7], which can then be modified with the time-varying values and solved at each time step to minimize computational overhead of the entire system. The use of advanced factorization techniques [38], [39] will become particularly important for larger networks. On the positive side, the solution obtained by the VBR model using the same time step will be more accurate, which may often justify the extra computational effort.

A more detailed analysis of the impact of using the VBR or PD models may be carried out using several typical systems (perhaps at least two—one with small proportion on machines and another with many machines). When conducting such studies, in addition to comparing the CPU cost per-time-step, one should also consider that both PD and VBR models permit much larger time-step and/or better accuracy (see Fig. 6), which is an advantage that was not utilized in [14] and should be fully exploited. Further investigation into this matter is of definite interest and significance that may be properly addressed in a dedicated publication.

VIII. Conclusion

This paper presented a VBR synchronous machine model for the nodal analysis method and EMTP-type programs. The VBR model interface with the electric network is non-iterative, and simultaneous solution of the machine variables and the network variables is achieved similar to the known PD model. Case studies of a single-machine, infinite-bus system demonstrate that the proposed model has computational advantages over the existing EMTP machine models.

Appendix A

See (A1)–(A10) at the bottom of this page and the top of the following page.

$$\mathbf{E}_1 = \begin{bmatrix} 2-\Delta tb_{11} & -\Delta tb_{12} \\ -\Delta tb_{21} & 2-\Delta tb_{22} \end{bmatrix}^{-1} \begin{bmatrix} \Delta tb_{13} \\ \Delta tb_{23} \end{bmatrix} \tag{A1}$$

$$\mathbf{E}_2 = \begin{bmatrix} 2-\Delta tb_{11} & -\Delta tb_{12} \\ -\Delta tb_{21} & 2-\Delta tb_{22} \end{bmatrix}^{-1} \begin{bmatrix} 2+\Delta tb_{11} & \Delta tb_{12} \\ \Delta tb_{21} & 2+\Delta tb_{22} \end{bmatrix} \tag{A2}$$

$$\mathbf{F}_1 = \begin{bmatrix} 2-\Delta tb_{31} & -\Delta tb_{32} \\ -\Delta tb_{41} & 2-\Delta tb_{42} \end{bmatrix}^{-1} \begin{bmatrix} \Delta tb_{33} \\ \Delta tb_{43} \end{bmatrix} \tag{A3}$$

$$\mathbf{F}_2 = \begin{bmatrix} 2-\Delta tb_{31} & -\Delta tb_{32} \\ -\Delta tb_{41} & 2-\Delta tb_{42} \end{bmatrix}^{-1} \begin{bmatrix} 2+\Delta tb_{31} & \Delta tb_{32} \\ \Delta tb_{41} & 2+\Delta tb_{42} \end{bmatrix} \tag{A4}$$

$$\mathbf{F}_3 = \begin{bmatrix} 2-\Delta tb_{31} & -\Delta tb_{32} \\ -\Delta tb_{41} & 2-\Delta tb_{42} \end{bmatrix}^{-1} \begin{bmatrix} 2\Delta t \\ 0 \end{bmatrix} \tag{A5}$$

$$b_{11} = \frac{r_{kq1}}{L_{lkq1}}\left(\frac{L''_{mq}}{L_{lkq1}} - 1\right); \quad b_{12} = \frac{r_{kq1}L''_{mq}}{L_{lkq1}L_{lkq2}}; \quad b_{13} = \frac{r_{kq1}L''_{mq}}{L_{lkq1}}$$

$$b_{21} = \frac{r_{kq2}L''_{mq}}{L_{lkq1}L_{lkq2}}; \quad b_{22} = \frac{r_{kq2}}{L_{lkq2}}\left(\frac{L''_{mq}}{L_{lkq2}} - 1\right); \quad b_{23} = \frac{r_{kq2}L''_{mq}}{L_{lkq2}}$$

$$b_{31} = \frac{r_{fd}}{L_{lfd}}\left(\frac{L''_{md}}{L_{lfd}} - 1\right); \quad b_{32} = \frac{r_{fd}L''_{md}}{L_{lfd}L_{lkd}}; \quad b_{33} = \frac{r_{fd}L''_{md}}{L_{lfd}}$$

$$b_{41} = \frac{r_{kd}L''_{md}}{L_{lfd}L_{lkd}}; \quad b_{42} = \frac{r_{kd}}{L_{lkd}}\left(\frac{L''_{md}}{L_{lkd}} - 1\right); \quad b_{43} = \frac{r_{kd}L''_{md}}{L_{lkd}}$$

$$\mathbf{k}_1(\omega_t) = \begin{bmatrix} c_{11} & c_{12} \\ c_{21}(\omega_r) & c_{22}(\omega_r) \end{bmatrix} \mathbf{E}_1 + \begin{bmatrix} c_{15} \\ 0 \end{bmatrix} \tag{A6}$$

$$\mathbf{k}_2(\omega_r) = \begin{bmatrix} c_{13}(\omega_r) & c_{14}(\omega_r) \\ c_{23} & c_{24} \end{bmatrix} \mathbf{F}_1 + \begin{bmatrix} 0 \\ c_{25} \end{bmatrix} \tag{A7}$$

$$\begin{aligned} \mathbf{h}_{qdr}(t) = & \begin{bmatrix} c_{11} & c_{12} \\ c_{21}(\omega_r) & c_{22}(\omega_r) \end{bmatrix} \mathbf{E}_2 \begin{bmatrix} \lambda_{kq1}(t-\Delta t) \\ \lambda_{kq2}(t-\Delta t) \end{bmatrix} \\ & + \begin{bmatrix} c_{11} & c_{12} \\ c_{21}(\omega_r) & c_{22}(\omega_r) \end{bmatrix} \mathbf{E}_1 i_{qs}(t-\Delta t) \\ & + \begin{bmatrix} c_{13}(\omega_r) & c_{14}(\omega_r) \\ c_{23} & c_{24} \end{bmatrix} \mathbf{F}_2 \begin{bmatrix} \lambda_{fd}(t-\Delta t) \\ \lambda_{kd}(t-\Delta t) \end{bmatrix} \\ & + \begin{bmatrix} c_{13}(\omega_r) & c_{14}(\omega_r) \\ c_{23} & c_{24} \end{bmatrix} \mathbf{F}_1 i_{ds}(t-\Delta t) \\ & + \left(\begin{bmatrix} c_{13}(\omega_r) & c_{14}(\omega_r) \\ c_{23} & c_{24} \end{bmatrix} \mathbf{F}_3 + \begin{bmatrix} 0 \\ c_{26} \end{bmatrix} \right) v_{fd} \end{aligned} \tag{A8}$$

$$c_{11} = \frac{L''_{mq} r_{kq1}}{L^2_{lkq1}} \left(\frac{L''_{mq}}{L_{lkq1}} - 1 \right) + \frac{L''_{mq} r_{kq2}}{L^2_{lkq2} L_{lkq1}}$$

$$c_{12} = \frac{L''_{mq} r_{kq2}}{L^2_{lkq2}} \left(\frac{L''_{mq}}{L_{lkq2}} - 1 \right) + \frac{L''^2_{mq} r_{kq1}}{L^2_{lkq1} L_{lkq2}}$$

$$c_{21}(\omega_r) = \frac{-\omega_r L''_{mq}}{L_{lkq1}}; \quad c_{22}(\omega_r) = \frac{-\omega_r L''_{mq}}{L_{lkq2}}$$

$$c_{13}(\omega_r) = \frac{\omega_r L''_{md}}{L_{lfd}}; \quad c_{14}(\omega_r) = \frac{\omega_r L''_{md}}{L_{lkd}}$$

$$c_{23} = \frac{L''_{md} r_{fd}}{L^2_{lfd}} \left(\frac{L''_{md}}{L_{lfd}} - 1 \right) + \frac{L''^2_{md} r_{kd}}{L^2_{lkd} L_{lfd}}$$

$$c_{24} = \frac{L''_{md} r_{kd}}{L^2_{lkd}} \left(\frac{L''_{md}}{L_{lkd}} - 1 \right) + \frac{L''^2_{md} r_{fd}}{L^2_{lfd} L_{lkd}}$$

$$c_{15} = \left(\frac{r_{kq1}}{L^2_{lkq1}} + \frac{r_{kq2}}{L^2_{lkq2}} \right) L''^2_{mq}; \quad c_{25} = \left(\frac{r_{fd}}{L^2_{lfd}} + \frac{r_{kd}}{L^2_{lkd}} \right) L''^2_{md}$$

$$c_{26} = \frac{L''_{md}}{L_{lfd}}$$

$$\mathbf{\Phi}^{pd}\left(\Delta t, t, \mathbf{x}^{pd}_{n-1}\right) = \begin{bmatrix} \mathbf{R}_s + \frac{2}{\Delta t}\mathbf{L}_s(t) & \frac{2}{\Delta t}\mathbf{L}_{sr}(t) \\ \frac{2}{\Delta t}\mathbf{L}_{rs}(t) & \mathbf{R}_r + \frac{2}{\Delta t}\mathbf{L}_r \end{bmatrix}^{-1} \begin{bmatrix} -\mathbf{R}_s + \frac{2}{\Delta t}\mathbf{L}_s(t-\Delta t) & \frac{2}{\Delta t}\mathbf{L}_{sr}(t-\Delta t) \\ \frac{2}{\Delta t}\mathbf{L}_{rs}(t-\Delta t) & -\mathbf{R}_r + \frac{2}{\Delta t}\mathbf{L}_r \end{bmatrix} \tag{A9}$$

$$\begin{aligned} \mathbf{\Phi}^{vbr}\left(\Delta t, t, \mathbf{x}^{vbr}_{n-1}\right) = & \begin{bmatrix} \mathbf{R}_s + \frac{2}{\Delta t}\mathbf{L}''_{abcs}(t) + \mathbf{M}_2(t) & \mathbf{M}_1(t) \\ -\begin{bmatrix} \mathbf{E}_1 & 0_{2\times1} & 0_{2\times1} \\ 0_{2\times1} & \mathbf{F}_1 & 0_{2\times1} \end{bmatrix} \mathbf{K}^r_s(t) & \mathbf{I}_{4\times4} \end{bmatrix}^{-1} \\ & + \begin{bmatrix} -\mathbf{R}_s + \frac{2}{\Delta t}\mathbf{L}_s(t-\Delta t) - \mathbf{M}_2(t-\Delta t) & -\mathbf{M}_1(t-\Delta t) \\ \begin{bmatrix} \mathbf{E}_1 & 0_{2\times1} & 0_{2\times1} \\ 0_{2\times1} & \mathbf{F}_1 & 0_{2\times1} \end{bmatrix} \mathbf{K}^r_s(t-\Delta t) & \begin{bmatrix} \mathbf{E}_1 & 0_{2\times1} \\ 0_{2\times1} & \mathbf{F}_2 \end{bmatrix} \end{bmatrix} \end{aligned} \tag{A10}$$

$$\mathbf{M}_1(t) = [\mathbf{K}^r_s(t)]^{-1} \begin{bmatrix} c_{11} & c_{12} & c_{13}(\omega_r) & c_{14}(\omega_r) \\ c_{21}(\omega_r) & c_{22}(\omega_r) & c_{23} & c_{24} \\ 0 & 0 & 0 & 0 \end{bmatrix}$$

$$\mathbf{M}_2(t) = [\mathbf{K}^r_s(t)]^{-1} \begin{bmatrix} c_{15} & 0 & 0 \\ 0 & c_{25} & 0 \\ 0 & 0 & 0 \end{bmatrix} \mathbf{K}^r_s(t).$$

APPENDIX B

Synchronous machine parameters [30]: 835 MVA, 26 kV, 0.85 pf, 2 poles, 3600 r/min, $J = 0.0658 \times 10^6$ J $\cdot$ s^2, $r_s = 0.00243\ \Omega$, $X_{ls} = 0.1538\ \Omega$, $X_q = 1.457\ \Omega$, $r_{kq1} = 0.00144\ \Omega$, $X_{lkq1} = 0.6578\ \Omega$, $r_{kq2} = 0.00681\ \Omega$, $X_{lkq2} = 0.07602\ \Omega$, $X_d = 1.457\ \Omega$, $r_{fd} = 0.00075\ \Omega$, $X_{lfd} = 0.1145\ \Omega$, $r_{kd} = 0.0108\ \Omega$, and $X_{lkd} = 0.06577\ \Omega$.

ACKNOWLEDGMENT

The authors would like to thank their UBC and Purdue colleagues Drs. H. W. Dommel, J. R. Marti, and S. D. Pekarek for

providing the inspiration for this paper. The authors also would like to especially thank H. W. Dommel for numerous discussions, including the impact of nonlinear and/or time-varying elements on the EMTP solution and for sharing with them the details of the MicroTran program.

REFERENCES

[1] P. Kundur, *Power System Stability and Control*. New York: McGraw-Hill, 1994, ch. 5.
[2] H. W. Dommel, *EMTP Theory Book*. Vancouver, BC, Canada: MicroTran Power System Analysis Corporation, 1992, ch. 8.
[3] Simulink Dynamic System Simulation Software—Users Manual. Natick, MA, MathWorks, 2005.
[4] Advanced Continuous Simulation Language (ACSL) Reference Manual. Concord, MA, Mitchell and Gauthier Associates, 1995.
[5] O. Wasynczuk and S. D. Sudhoff, "Automated state model generation algorithm for power circuits and systems," *IEEE Trans. Power Syst.*, vol. 11, no. 4, pp. 1951–1956, Nov. 1996.
[6] H. W. Dommel, "Digital computer solution of electromagnetic transients in single- and multiphase networks," *IEEE Trans. Power App. Syst.*, vol. PAS-88, no. 4, pp. 388–399, Apr. 1969.
[7] L. W. Nagel and D. O. Pederson, *Simulation Program With Integrated Circuit Emphasis*. Berkeley: Univ. California Electronic Research Laboratory, 1973.
[8] V. Brandwajn, "Synchronous generator models for the analysis of electromagnetic transients," Ph.D. dissertation, Univ. British Columbia, Vancouver, BC, Canada, 1977.
[9] MicroTran Power Reference Manual. Vancouver, BC, Canada, MicroTran Power System Analysis Corp., 1997.
[10] Electromagnetic Transient Programs (EMTP96) Rule Book I, EMTP Development Coordination Group (DCG) and Electric Power Research Institute (EPRI), Inc., 1999.
[11] H. K. Lauw and W. S. Meyer, "Universal machine modeling for the representation of rotating electrical machinery in an electromagnetic transients program," *IEEE Trans. Power App. Syst.*, vol. PAS-101, pp. 1342–1351, 1982.
[12] *EMTDC User's Guide*. Winnipeg, MB, Canada: Manitoba HVDC Research Center Inc., 2004, ch. 8.
[13] A. M. Gole, R. W. Menzies, D. A. Woodford, and H. Turanli, "Improved interfacing of electrical machine models in electromagnetic transient programs," *IEEE Trans. Power App. Syst.*, vol. PAS-103, no. 9, pp. 2446–2451, Sep. 1984.
[14] X. Cao, A. Kurita, H. Mitsuma, Y. Tada, and H. Okamoto, "Improvements of numerical stability of electromagnetic transient simulation by use of phase-domain synchronous machine models," *Elect. Eng. Jpn.*, vol. 128, no. 3, pp. 53–62, Apr. 1999.
[15] A. B. Dehkordi, A. M. Gole, and T. L. Maguire, "Permanent magnet synchronous machine model for real-time simulation," in *Proc. Interracial Conf. Power Systems Transients*, Montreal, QC, Canada, Jun. 2005.
[16] J. Hollman and J. Marti, "Real time network simulation with PC—Cluster," *IEEE Trans. Power Syst.*, vol. 18, no. 2, pp. 563–569, May 2003.
[17] P. Subramaniam and O. P. Malik, "Digital simulation of a synchronous generator in the direct-phase quantities," *Proc. Inst. Elect. Eng.*, vol. 118, no. 1, pp. 153–160, Jan. 1971.
[18] M. Rafian and M. A. Laughton, "Determination of synchronous machine phase coordinate parameters," *Proc. Inst. Elect. Eng.*, vol. 123, no. 8, pp. 818–824, Aug. 1976.
[19] J. R. Marti and K. W. Louie, "A phase-domain synchronous generator model including saturation effects," *IEEE Trans. Power Syst.*, vol. 12, no. 1, pp. 222–229, Feb. 1997.
[20] D. Muthumuni, P. G. McLaren, E. Dirks, and V. Pathirana, "A synchronous machine model to analyze internal faults," in *Proc. IEEE Industry Application Conf., 36th IAS Annu. Meeting*, Oct. 2001, vol. 3, pp. 1595–1600.
[21] New S.M. Model from Tokyo Electric. [Online]. Available: http://www.jaug.jp/~atp/index-e.htm.
[22] Can/Am EMTP News, Voice of the Canadian/American EMTP User Group, 1997, vol. 97-2.
[23] Can/Am EMTP News, Voice of the Canadian/American EMTP User Group, 1999, vol. 99-3.
[24] W. Gao, E. V. Solodovnik, and R. A. Dougal, "Symbolically aided model development for an induction machine in virtual test bed," *IEEE Trans. Energy Convers.*, vol. 19, no. 1, pp. 125–135, Mar. 2004.
[25] S. D. Pekarek, O. Wasynczuk, and H. J. Hegner, "An efficient and accurate model for the simulation and analysis of synchronous machine/converter systems," *IEEE Trans. Energy Convers.*, vol. 13, no. 1, pp. 42–48, Mar. 1998.
[26] W. Zhu, S. D. Pekarek, J. Jatskevich, O. Wasynczuk, and D. Delisle, "A model-in-the-loop interface to emulate source dynamics in a zonal DC distribution system," *IEEE Trans. Power Electron.*, vol. 20, no. 2, pp. 438–445, Mar. 2005.
[27] J. R. Marti, L. R. Linares, J. Calvino, H. W. Dommel, and J. Lin, "OVNI: An object approach to real-time power system simulators," in *Proc. Int. Conf. Power System Technology*, Beijing, China, Apr. 1998, pp. 977–981.
[28] S. D. Pekarek, O. Wasynczuk, E. A. Walters, J. Jatskevich, C. E. Lucas, N. Wu, and P. T. Lamm, "An efficient multi-rate simulation technique for power-electronic-based systems," *IEEE Trans. Power Syst.*, vol. 19, no. 1, pp. 399–409, Feb. 2004.
[29] F. A. Moreira and J. R. Marti, "Latency techniques for time-domain power system transients simulation," *IEEE Trans. Power Syst.*, vol. 20, no. 1, pp. 246–253, Feb. 2005.
[30] P. C. Krause, O. Wasynczuk, and S. D. Sudhoff, *Analysis of Electric Machinery and Drive Systems*, 2nd ed. Piscataway, NJ: IEEE Press, 2002.
[31] S. Boyd and L. Vandenberghe, *Convex Optimization*. Cambridge, U.K.: Cambridge Univ. Press, 2004, pp. 662–664.
[32] L. Wang, J. Jatskevich, and H. W. Dommel, "Reexamination of synchronous machine modeling techniques for EMTP simulations," *IEEE Trans. Power Syst.*, submitted for publication.
[33] W. Gautchi, *Numerical Analysis: An Introduction*. Boston, MA: Birkhauser, 1997.
[34] R. A. DeCarlo, *Linear Systems: A State Variable Approach With Numerical Implementation*. Englewood Cliffs, NJ: Prentice-Hall, 1989, pp. 457–457.
[35] L. O. Chua and P.-M. Lin, *Computer Aided Analysis of Electronic Circuit: Algorithms and Computational Techniques*. Englewood Cliffs, NJ: Prentice-Hall, 1975, pp. 43–45.
[36] Private Notes and Discussions With H. W. Dommel Univ. British Columbia. Vancouver, BC, Canada, Jul. 2006.
[37] "First benchmark model for computer simulation of subsynchronous resonance," *IEEE Trans. Power App. Syst.*, vol. PAS-96, pp. 1565–1572, Sep./Oct. 1977.
[38] H. W. Dommel, "Nonlinear and time-varying elements in digital simulation of electromagnetic transients," *IEEE Trans. Power App. Syst.*, vol. PAS-90, pp. 2561–2567, Nov./Dec. 1971.
[39] S. M. Chan and V. Brandwajn, "Partial matrix refactorization," *IEEE Trans. Power App. Syst.*, vol. PWRS-1, no. 1, pp. 193–200, Feb. 1986.

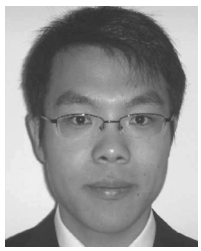

Liwei Wang (S'04) received the M.S. degree in electrical engineering from Tianjin University, Tianjin, China, in 2004. He is currently pursuing the Ph.D. degree in electrical and computer engineering at the University of British Columbia, Vancouver, BC, Canada.

His research interests include electrical machines, power, and power electronic systems simulation.

Juri Jatskevich (M'99) received the M.S.E.E. and Ph.D. degrees from Purdue University, West Lafayette, IN, in 1997 and 1999, respectively.

He was with Purdue, as well as consulting for P. C. Krause and Associates, Inc,. until 2002. Since 2002, he has been an Assistant Professor of electrical and computer engineering at the University of British Columbia, Vancouver, BC, Canada. His research interests include electrical machines, power electronic systems, and simulation.